24

MEMS Tunable Resonant Leaky-Mode Filters for Multispectral Imaging Applications

Robert Magnusson and Mehrdad Shokooh-Saremi
University of Texas at Arlington, Department of Electrical Engineering
USA

1. Introduction

Multispectral imaging refers to a combination of spectroscopy and photography. By using rapidly tunable filters and two-dimensional (2D) image planes such as those provided by charge-coupled device (CCD) detectors, data sets containing spatial (x, y) and spectral information are acquired. The resulting spectral image cubes contain intensity and wavelength (λ) data at each pixel in the 2D image (Gat, 2000). Under time-varying conditions, the data cube would be multidimensional in (x, y, λ, t) space. Hyperspectral imaging is a similar concept principally differentiated from multispectral imaging in that many more wavelengths and narrower spectral passbands are employed. Thus, in multispectral imaging, relatively few wavelengths are used to carry the spatial information, whereas in hyperspectral imaging, the number of wavelength channels may reach ~100 (Vo-Dinh et al., 2004). Each of these methods is connected with a plethora of useful applications. Examples include spatio-spectral diagnostics in agricultural crop management, true-color night vision, forensics, and archaeology and art (Gat, 2000). In medicine, hyperspectral in-vivo diagnostics of tissue may avoid excision and permit in situ analysis (Vo-Dinh et al., 2004). Its application to real-time guidance in surgery is promising (Vo-Dinh et al., 2004).
The capability of the tunable filters central to these spectral imaging methods defines the quality of the data sets collected. Gat lists principal attributes of ideal tunable filters and describes examples of filters employed to date (Gat, 2000). Among these, tunable liquid-crystal and acousto-optical filters represent two prominent device classes (Gat, 2000; Vo-Dinh et al., 2004). The former is based on stacks of birefringent liquid-crystal plates integrated with polarizers, whereas the latter is diffractive in nature.
In the present contribution, we introduce a new tunable filter concept for potential application in multispectral and hyperspectral imaging systems. In short, we employ a resonant waveguide grating supporting leaky modes that is tuned by micro-electro-mechanical (MEMS) means. We begin this chapter by summarizing the physical basis for this class of tunable filters. Then, we provide numerical spectral characteristics of resonance elements based on exact electromagnetic models of the devices with representative materials. We investigate theoretically the operation of MEMS-tunable resonant elements.

Based on "Tunable Leaky-Mode MEMS Filters for Multispectral Imaging Applications," by R. Magnusson and M. Shokooh-Saremi, which appeared in IEEE Aerospace Conference Proceedings, March 1-8, 2008.

Source: Aerospace Technologies Advancements, Book edited by: Dr. Thawar T. Arif,
ISBN 978-953-7619-96-1, pp. 492, January 2010, INTECH, Croatia, downloaded from SCIYO.COM

In particular, we provide numerical results for a fixed transmission filter, a tunable reflection filter mounted on a low-index substrate, and then contrast its tuning capability with that of a classical Fabry-Perot filter in the LWIR band. Further examples of guided-mode resonance (GMR) tunable devices for multispectral imaging applications quantify their tunability relative to the mechanical displacement as well as spectral bandwidths and associated sideband levels. We envision these tunable filters finding use in aerospace multispectral imaging applications such as multi-channel thermal imaging, landscape temperature mapping, remote sensing, multispectral IR target recognition, and in other areas.

2. Resonance principle and context

Subwavelength periodic elements are presently of immense interest owing to their applicability in numerous optical systems and devices including biosensors, lasers, and filters. When the lattice is confined to a layer, thereby forming a periodic waveguide, an incident optical wave may undergo a guided-mode resonance (GMR) on coupling to a leaky eigenmode of the layer system. The external spectral signatures can have complex shapes with high efficiencies in both reflection and transmission. Computed examples in the optical spectral region show that subwavelength periodic leaky-mode waveguide films provide diverse spectral characteristics such that even single-layer elements can function as narrow-line bandpass filters, polarized wideband reflectors, wideband polarizers, polarization-independent elements, and wideband antireflection films (Ding & Magnusson, May 2004; Ding & Magnusson, November 2004). The relevant physical properties of these elements can be explained in terms of the structure of the second (leaky) photonic stopband and its relation to the symmetry of the periodic profile. The interaction dynamics of the leaky modes at resonance contribute to sculpting the spectral bands. The leaky-mode spectral placement, their spectral density, and their levels of interaction decisively affect device operation and associated functionality (Ding & Magnusson, May 2004; Ding & Magnusson, November 2004). In this paper, we investigate the tuning properties of a grating resonance element in which mechanical motion alters the structural symmetry. The chief properties of example tunable micro-electro-mechanical (MEMS) devices are summarized. This work initiates development of multispectral pixels operating in spectral regions where no comparable studies have been conducted to date.

GMR device parameters, including refractive index of grating layers or surrounding media, thickness, period, and fill factor, can all be applied to implement tunability. In past publications, a tunable laser using a rotating resonance element (i.e., angular tuning) and a photorefractive tunable filter were described (Wang & Magnusson, 1993). Furthermore, tuning can be accomplished by changing layer thickness or material refractive index, a method of significance in resonant sensor operation (Magnusson & Wang, 1993). Suh et al. reported analysis of a tunable structure consisting of two adjacent photonic-crystal films, each composing a two-dimensional waveguide grating, which could be displaced laterally or longitudinally by a mechanical force (Suh et al., 2003). Each periodic waveguide admitted guided-mode resonances whose coupling could be mechanically altered for spectral tuning. Additionally, numerous other tunable structures not inducing leaky modes have been described in the literature. As an example of a device in this class, Nakagawa and Fainman presented a structure in which a subwavelength grating was placed between planar dielectric mirrors, composing a Fabry-Perot cavity (Nakagawa & Fainman, 2004). Lateral and longitudinal motion yielded effective tuning via associated near-field coupling mechanisms. Park and Lee presented a tunable nanophotonic grating layer that was placed

on a flexible substrate (Park & Lee, 2004). By mechanically stretching the lattice, thereby changing the grating period, a variation in the angle of refraction of an incident beam of light was achieved.

Previously, we presented the characteristics of MEMS-tunable guided-mode resonance structures in the telecommunications spectral band and explained their operational principles. It was shown that such systems are highly tunable with only nanoscale displacements needed for wide-range tuning. Working with a single-example materials system, namely silicon-on-insulator (SOI), and fixed parameters, we quantified the level of tunability per unit movement for an example resonant structure. It was found that effective MEMS-based tuning can be accomplished by variation of grating profile symmetry, by changing the waveguide thickness, or both (Magnusson & Ding, 2006). Clearly, analogous tunable devices can be made in numerous other materials systems and made to operate in arbitrary spectral regions. As the operational wavelength diminishes to the visible region, the associated finer-feature patterning demands stricter tolerances in fabrication. Conversely, for the MWIR and LWIR bands, the structural features increase in size, relaxing fabrication tolerances.

3. Resonance device classes

In this section, we present examples of optical filters with distinct features and performance. A fixed guided-mode resonance element provides a narrow bandpass filter centered at 10 μm wavelength. A tunable bandstop filter fashioned with substrate-mounted complementary gratings is MEMS-tuned in the same spectral region. Finally, the tuning capability of a classical multilayered Fabry-Perot cavity is assessed for comparison and contrast with the GMR MEMS filters.

Narrow-line bandpass filter for the LWIR band – Bandpass filters are widely used to filter spectra into narrow wavelength bands typically in transmission geometry. Here, a narrowband filter based on leaky-mode resonance is designed with the particle swarm optimization (PSO) technique and its transmittance is determined (Shokooh-Saremi & Magnusson, 2007). Figure 1 shows the structural details of the device. This device consists of a subwavelength (namely, there exists no higher-order, freely propagating diffracted waves) grating whose period has been divided into four parts. The fraction of the period occupied by each medium is defined by the corresponding fill factor F_i. Figure 2 shows the

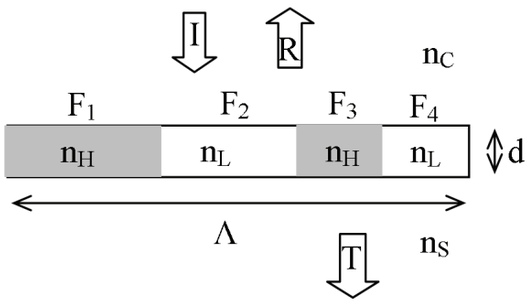

Fig. 1. Structure of a four-part GMR device used for designing a narrow bandpass filter. Λ, d denote the period and thickness of the grating, respectively, whereas n_C and n_S define the refractive indices of the cover and substrate media. Also, n_H and n_L are the refractive indices of materials in the grating region ($n_H > n_L$). The fractions F_i (i=1,2,3,4) denote the associated fill factors. R is reflectance, and T is transmittance.

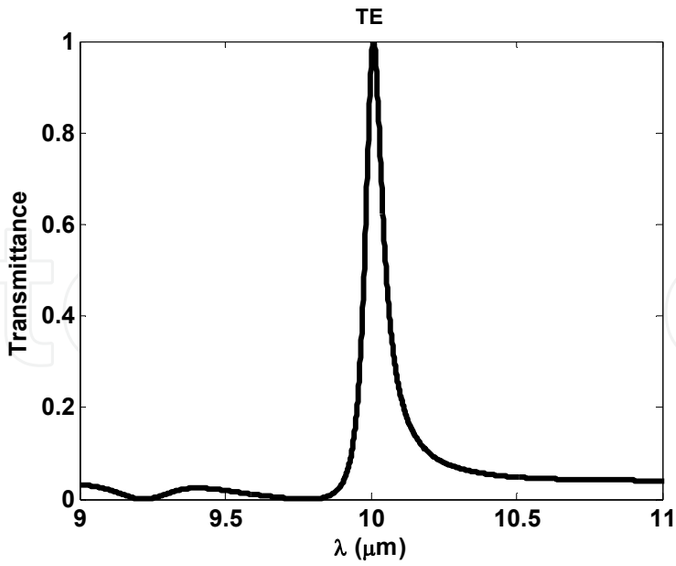

Fig. 2. Transmittance spectrum of a narrow bandpass filter designed by PSO for TE polarization (electric field vector normal to the plane of incidence). The period is Λ = 6.57 μm, thickness d = 5.93 μm and $\{F_1,F_2,F_3,F_4\}$ = {0.137,0.177,0.372,0.314}. Also, $n_C = n_S = n_L = 1.0$ and n_H = 3.42 (Si).

transmittance spectrum of the PSO-designed filter for normal incidence and TE polarization. The final design parameters are: Λ = 6.57 μm, d = 5.93 μm, and $\{F_1,F_2,F_3,F_4\}$ ={0.137,0.177,0.372,0.314}. Also, $n_C = n_S = n_L = 1.0$ (membrane structure) and n_H = 3.42 (Si). This filter has a transmission band of ~ 0.1 μm around the λ = 10.0 μm central resonance wavelength. In the examples, silicon is used due to its high refractive index in the IR band; however, other applicable materials with high and low refractive indices in the LWIR band can be used in practical applications like Ge (n = 4.0), GaAs (n = 3.27), ZnSe (n = 2.4), NaCl (n = 1.5) and KCl (n = 1.46) (Janos).

In fabrication of elements of this class, the aspect ratio, namely the height-to-width ratio of each grating block is of key importance. In this example, the smallest aspect ratio is $d/F_1\Lambda$~6.6. Fabrication of this device would be possible with optical lithography and deep reactive-ion etching.

Tunable LWIR bandstop filter—Figure 3 shows a schematic diagram of a tunable structure that can be constructed with two silicon single-layer waveguide gratings, one of which would be mobile. The period, Λ, of the resonance structure in Fig. 3 is selected to implement tunability in the 8–12 μm wavelength range for TE polarization. Other parameters are selected such that an appreciable range of motion is available. The tuning parameters studied here are limited to the separation of the two binary Si blocks along the horizontal direction denoted by F_{tune} (dimensionless fill factor) and the separation of the two gratings along the vertical direction denoted by d_{tune}. The tuning with horizontal motion varies the symmetry of the grating profile by shifting a Si block within the period (Ding & Magnusson, May 2004; Magnusson & Ding, 2006). This alters the spatial configuration of the localized resonant fields, including relative position of standing-wave peaks and grating materials. The vertical motion changes the net thickness and also affects the resonance wavelength and leaky mode distribution. The horizontal and vertical translational parameters F_{tune} and d_{tune} can be applied simultaneously or independently. The simulation results show that the

tuning by horizontal movement is more effective than the vertical movement (Magnusson & Ding, 2006). MEMS technology and actuation methods can be applied to implement these tunable elements.

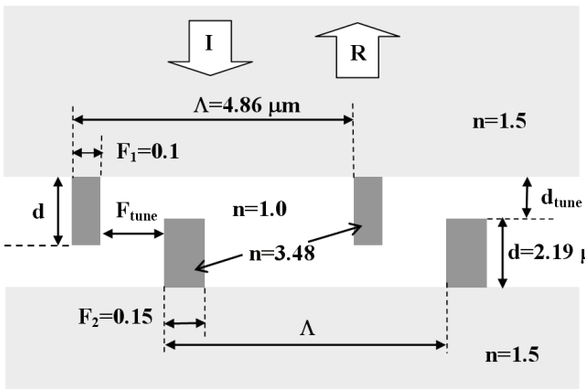

Fig. 3. An example tunable double-grating resonant structure. The gratings are made with silicon and supported on lower-index substrates. The incident wave is taken to be TE polarized.

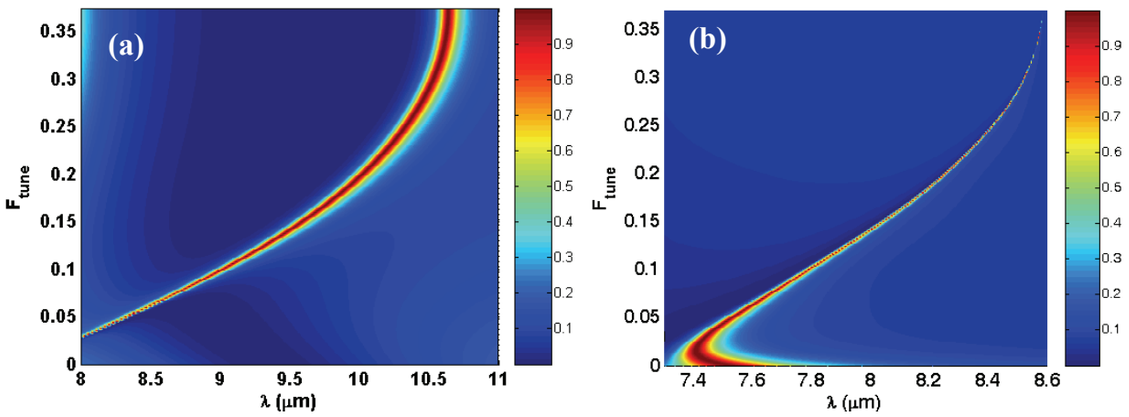

Fig. 4. Color-coded map illustration of resonance tuning $R_0(\lambda,F_{tune})$ by modulation of the profile symmetry while holding $d_{tune} = 0$ for (a) TE , and (b) TM polarizations. The incident angle is $\theta = 0°$.

Figure 4 provides a color-coded map of the reflectance of the zero-order wave $R_0(\lambda,F_{tune})$ that quantifies the spectral shift, lineshape, and linewidth of the resonance reflectance peak as a result of horizontal profile tuning for TE and TM polarizations. As seen, the tuning map for TM polarization falls outside of the 8–12 μm range; however, these two polarizations can provide a total tuning range of ~7.6–10.5 μm. Therefore, by utilizing a polarization switching method, wider spectral tuning range can be achieved. Figure 5 shows snapshots of the reflectance spectra for selected values of F_{tune} for TE polarization. In general, the peak shift is accompanied by linewidth change; in this case, the resonance linewidth increases as the peak shifts to longer wavelength within the range shown. It is seen that the resonance wavelength can be shifted by ~2.5 μm, from 8.0 μm to 10.5 μm, with a horizontal movement of ~1.7 μm. At $F_{tune} = 0.375$, the structure is symmetric, accounting for the reversal in wavelength shift at that point. Thus, for example, the physical situation for $F_{tune} = 0.05$ is the

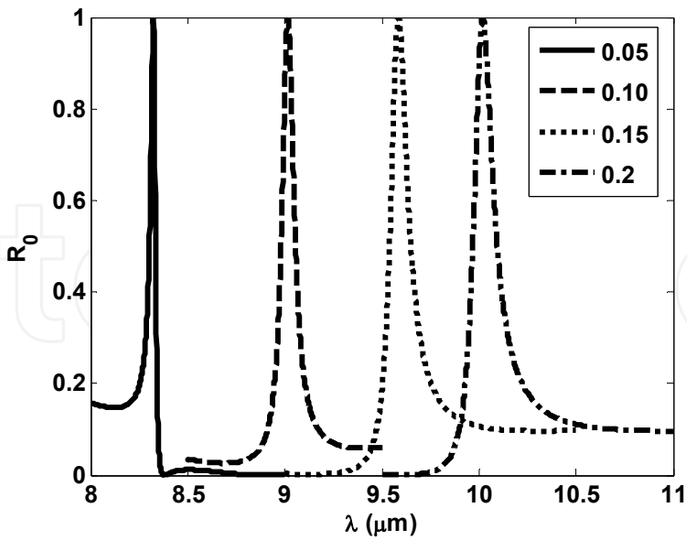

Fig. 5. Examples of reflectance spectra of the silicon double grating tunable filter for various values of F_{tune} for TE polarization. The zero-order reflectance is denoted by R_0.

same as that for F_{tune} = 0.70. Figure 6 shows the distribution of the total electric field inside the device and also the surrounding media at resonance for a given set of parameters. It is seen that the field amplitude in the Si blocks increases by ~×10 (F_{tune} = 0.20) over the input wave amplitude, which is one unit. Varying the symmetry tuning parameter, F_{tune}, alters the internal field distributions and their amplitudes as seen in Fig. 6.

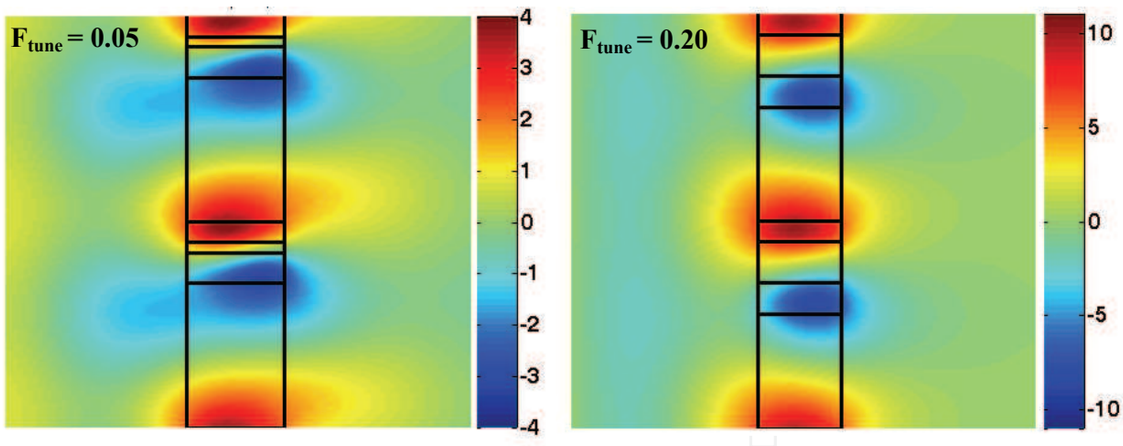

Fig. 6. Total electric field distribution patterns at resonance for two values of the symmetry parameter (TE polarization). The two counterpropagating leaky modes form a standing wave with a TE_0 mode shape at resonance. The incident wave has unit amplitude.

The spectral and modal results shown are obtained by rigorous coupled-wave analysis (RCWA) (Gaylord & Moharam, 1985) and modal analysis technique (Peng et al., 1975), respectively. Using these exact electromagnetic methods, the interaction of the incident light plane wave with general multilayered periodic devices is efficiently modeled. We have developed computer codes that handle general combinations of periodic and homogeneous

layered structures. Because of the plane-wave assumptions used, these codes run extremely fast and are found to be highly reliable as verified by repeated comparisons with experimental results. Additionally, coupled-wave field distributions, including resonant leaky-mode amplitudes as illustrated in examples above, can be conveniently and efficiently computed with RCWA and related methods.

Tunable Fabry-Perot filters — For context and to connect and contrast our methods with better known technology, we address briefly the properties of MEMS-tunable Fabry-Perot (FP) filters. Figure 7 shows the device details consisting of two quarter-wave Bragg stacks with 8 layers each surrounding a variable gap. Figure 8 shows the performance of the FP filter with

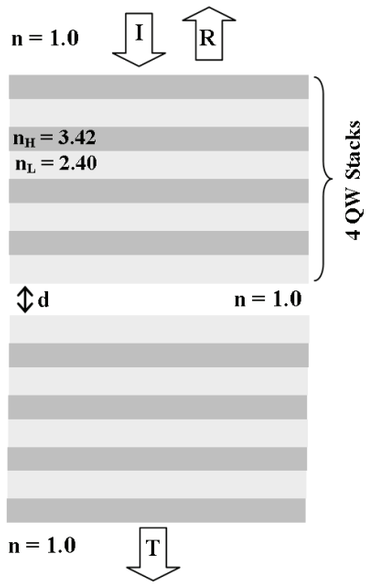

Fig. 7. A Fabry-Perot MEMS-tunable thin-film filter with variable gap operating in the in 8–12 μm band.

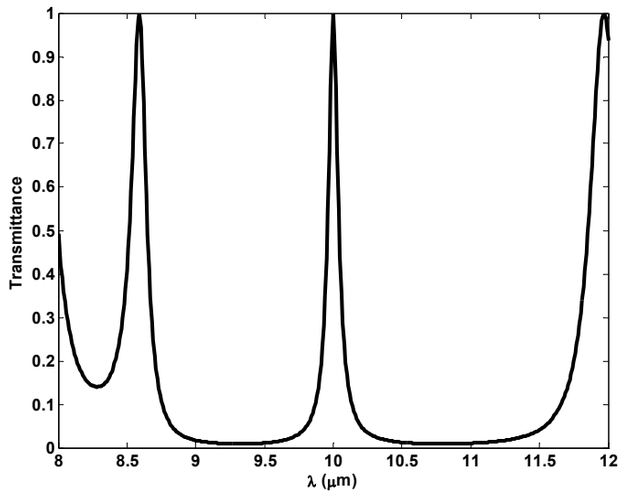

Fig. 8. FP filter transmission curve for example parameters that are $\theta = 0°$, $\lambda_0 = 10.0$ μm, $d_H = \lambda_0/4n_H = 0.731$ μm, $d_L = \lambda_0/4n_L = 1.04$ μm, and fixed air gap width of $d = 5.0$ μm.

representative parameters. Finally, Fig. 9 displays the tuning properties of the FP filter. Note that for a given gap width, say d = 5 μm, two transmission peaks arise in the 8–12 μm region. Thus, to eliminate extraneous transmissions, additional blocking (edge) filters are needed. The net result is that tuning is restricted by the parasitic neighboring resonance transmission channels as seen in the figure. In this example, spectral tuning across ~1 μm with gap change of ~5 μm is possible with proper blocking filters. This is to be compared with the tuning capability shown in Fig. 4 where a single resonance is encountered across a wide spectral band. This yields resonance wavelength change of ~2.5 μm with a movement of ~1.7 μm, which is considerably more effective.

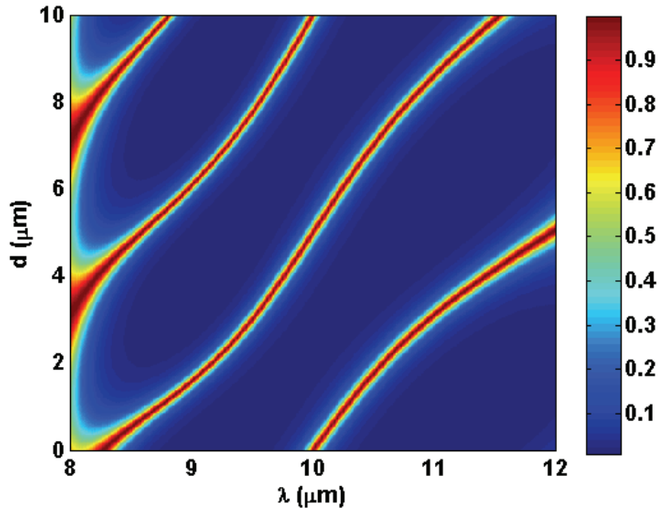

Fig. 9. FP filter performance under tuning by varying the gap dimension, d. The red bands define (d, λ) loci where the filter is highly transmissive.

4. Tunable membrane filter

In this section, a freestanding, tunable reflective pixel is introduced as a potential candidate for multispectral imaging applications. The device has a membrane structure in which the incident and substrate media are assumed to be air. The grating has four parts per period like the structure in Fig. 1. Figure 10 shows the structure of this tunable element. For simulating the action of the MEMS system for tuning the reflectance spectrum of the device, the air part with filling factor of F_2 is considered as being variable. This imitates the movement of the silicon part with filling factor F_3 by MEMS actuation as indicated in Fig. 10. The tunable imaging pixel has been designed to operate in the 8–12 μm band. The parameters of the device are as follows: Λ = 6.0 μm, d = 2.4 μm, F_1 = 0.15, F_3 = 0.1, and n_H = 3.42 (Si). Considering these parameters, Fig. 11 displays a color-coded map of $R_0(\lambda,F_2)$ illustrating the tuning of the resonance reflection spectrum. As seen in this figure, the pixel is tunable over the 9–12.4 μm range while the mechanical displacement needed for this tuning is ~0.373Λ = 2.24 μm. Therefore, the rate of tuning is ~1.52 (wavelength shift per mechanical shift). Also, Fig. 12 shows example snapshots of the spectrum for various values of F_2. This figure quantifies the resonance peak line shape, line width, and side lobe levels associated with this particular pixel.

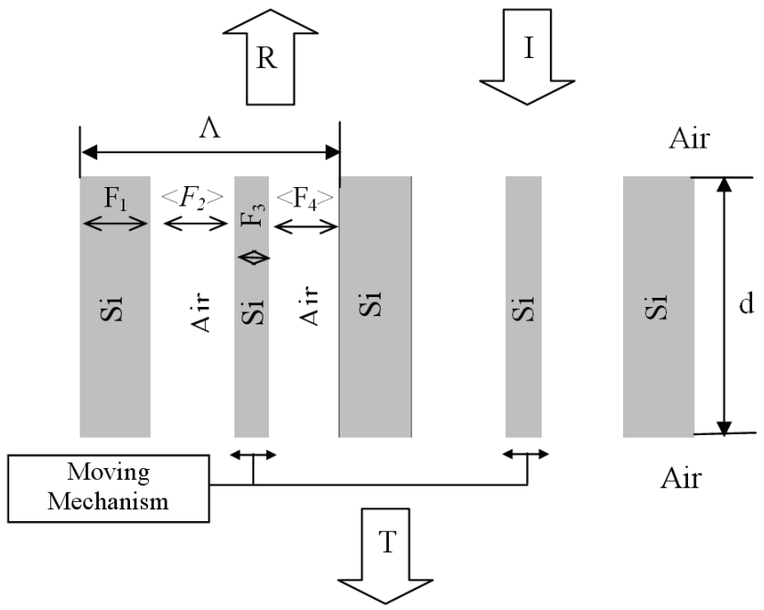

Fig. 10. Structure of a four-part GMR tunable membrane device. Λ, d are the period and thickness of the grating, respectively.

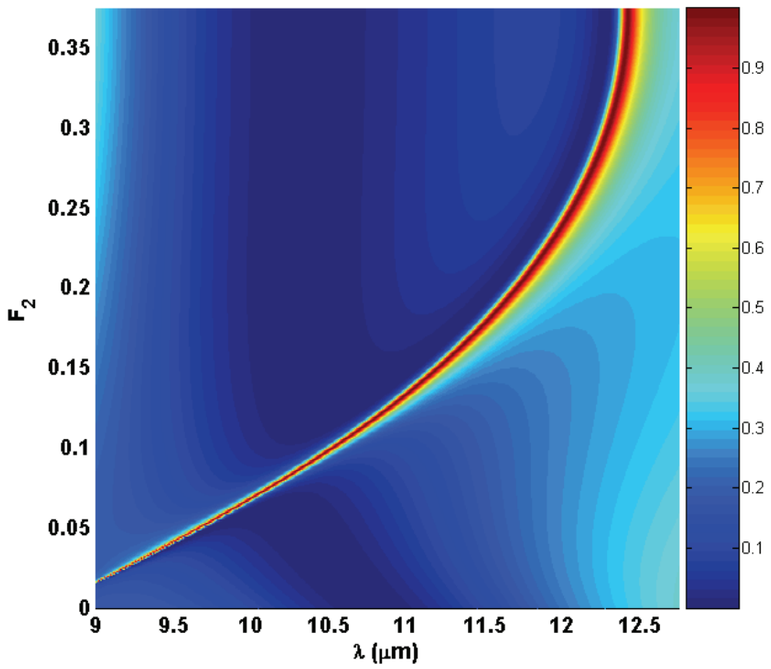

Fig. 11. Color-coded map of $R_0(\lambda,F_2)$ for the tunable MEMS pixel made with a silicon membrane. The parameters of the device are as follows: Λ = 6.0 μm, d = 2.4 μm, F_1 = 0.15, F_3 = 0.1, and n_H = 3.42 (Si).

To study the angular response of the tunable elements, the variation of the resonance peak reflectance versus angle of incidence has been calculated and the result is shown in Figure 13. The center wavelength is 10.52 μm, and F_2 is chosen to be 0.1. It is seen that a favorable

numerical aperture is available for these devices. At ±2.5° angular deviation, the reflectance of the resonance exceeds 0.9 and the FWHM of the spectrum is ~10°.

Since these elements work in reflection mode, practical arrangements are needed to suitably direct the reflected beam to the detection system (for example, detector arrays). Figure 14 illustrates two possible schematic detection arrangements. In Fig. 14(a), a beamsplitter cube is utilized to direct the reflected beam from the pixel element to the detector array. This arrangement is useful if the element is designed to work under normal incidence conditions. On the other hand, for pixel elements designed to work at oblique incidence, the arrangement in Fig. 14(b) is more appropriate.

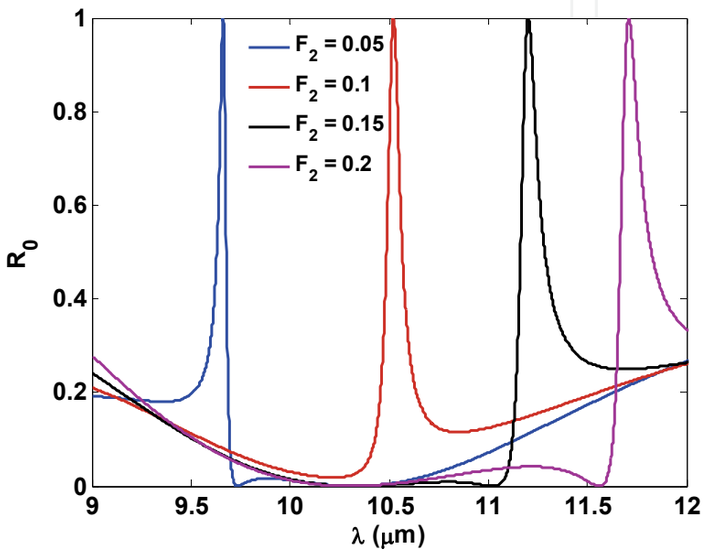

Fig. 12. Snapshots of reflection spectra for various values of F_2.

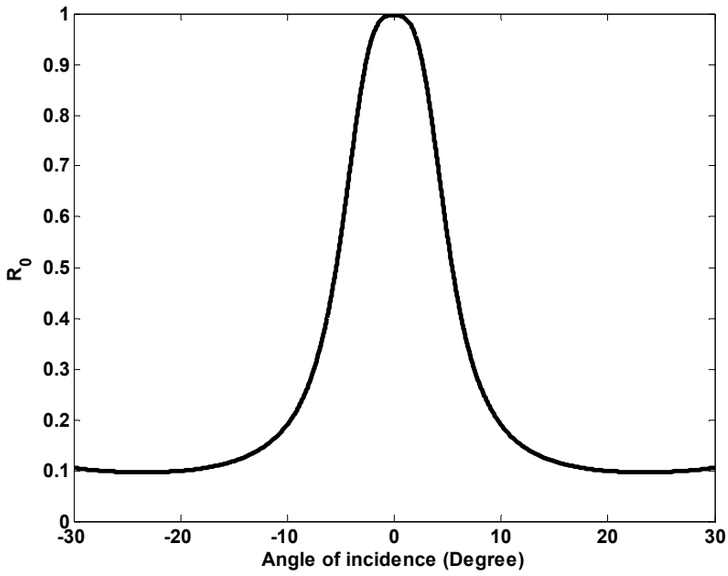

Fig. 13. Angular spectrum of the pixel element at λ = 10.52 μm and F_2 = 0.1.

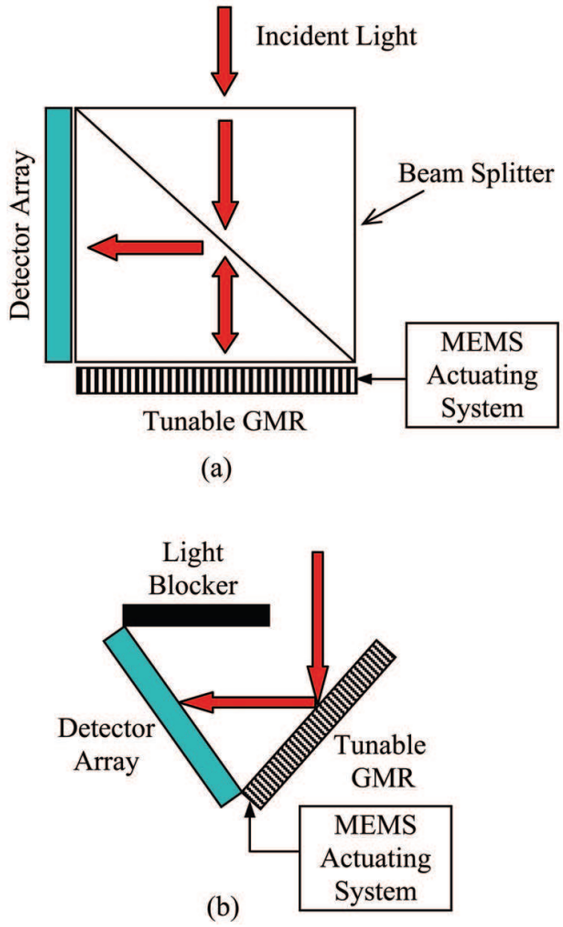

Fig. 14. Arrangements for reflected light detection from the tunable pixels under, (a) normal incidence and (b) oblique incidence.

5. Conclusions

In this paper, MEMS-tunable leaky mode structures have been investigated for applications in multispectral and hyperspectral imaging. It has been shown that high degrees of tunability can be achieved without parasitic neighboring spectral channels. Numerous computed examples of these devices have quantified their tunability relative to the mechanical displacement as well as spectral bandwidths and associated sideband levels. Particular example results for a silicon grating element with 6.0 μm period and 2.4 μm thickness show MEMS tuning of ~3.4 μm in the ~9–12 μm band and ~100 nm spectral resonance linewidth. We have previously studied analogous devices in the telecommunications region around 1.55 μm wavelength (Magnusson & Ding, 2006) and in the visible spectral region for use as display pixels (Magnusson & Shokooh-Saremi, 2007). For resonance devices operating in the MWIR and LWIR bands, the structural features increase in size relative to those in the short-wave regions, thereby relaxing fabrication tolerances to some degree. Using photolithography and deep reactive-ion etching, these filters can be fabricated in many common materials systems including silicon. Nevertheless, the high aspect ratios encountered in some cases demand high precision in fabrication.

High aspect ratios are particularly associated with small filling factors in the basic resonance gratings. Optimization in design to minimize aspect ratios while retaining high degrees of tuning remains a chief challenge. Experimental realization and characterization of MEMS-tuned LWIR multispectral elements is another interesting, future prospect.

6. References

Ding, Y. & Magnusson, R. (2004). Use of nondegenerate resonant leaky modes to fashion diverse optical spectra. *Opt. Express*, Vol. 12, No. 9, (May 2004) pp. 1885-1891, ISSN # 10944087

Ding, Y. & Magnusson, R. (2004). Resonant leaky-mode spectral-band engineering and device applications. *Opt. Express*, Vol. 12, No. 23, (November 2004) pp. 5661-5674, ISSN # 10944087

Gat, N. (April 2000). Imaging spectroscopy using tunable filters: A review, In: *Wavelet Applications VII*, Harold H. Szu, Martin Vetterli, William J. Campbell, James R. Buss, Eds., (Vol. 4056), pp. 50-64, SPIE, 0819436828, Bellingham, Wash

Gaylord, T. K. & Moharam, M. G. (1985). Analysis and applications of optical diffraction by gratings. *Proc. IEEE*, Vol. 73, No. 5, (May 1985) pp. 894-937, 00189219

Janos Technology, http://www.janostech.com

Magnusson, R. & Ding, Y. (2006). MEMS tunable resonant leaky mode filters. *IEEE Photonics Technol. Lett.*, Vol. 18, No. 13-16, (July 2006) pp. 1479-1481, 10411135

Magnusson, R. & Shokooh-Saremi, M. (2007). Widely tunable guided-mode resonance nanoelectromechanical RGB pixels. *Opt. Express*, Vol. 15, No. 17, (August 2007) pp. 10903-10910, ISSN # 10944087

Magnusson, R. & Wang, S. S. (1993). Optical guided-mode resonance filter. U.S. patent number 5,216,680, June 1, 1993

Nakagawa, W. & Fainman, Y. (2004). Tunable optical nanocavity based on modulation of near-field coupling between subwavelength periodic nanostructures," *IEEE J. Select. Topics Quantum Electron.*, Vol. 10, No. 3, (May/June 2004) pp. 478–483, 1077260X

Park, W. & Lee, J. B. (2004). Mechanically tunable photonic crystal structures. *Appl. Phys. Lett.*, Vol. 85, (November 2004) pp. 4845-4847, ISSN # 00036951

Peng, S. T.; Tamir, T. & Bertoni, H. L. (1975). Theory of periodic dielectric waveguides. *IEEE Trans. on Microwave Theory Tech.*, Vol. 23, No. 1, (January 1975) pp. 123-133, 00189480

Shokooh-Saremi, M. & Magnusson, R. (2007). Particle swarm optimization and its application to the design of diffraction grating filters. *Opt. Lett.*, Vol. 32, No. 8, (April 2007) pp. 894-896, 01469592

Suh, W.; Yanik, M. F.; Solgaard, O. & Fan, S. (2003). Displacement-sensitive photonic crystal structures based on guided resonances in photonic crystal slabs. *Appl. Phys. Lett.*, Vol. 82, (March 2003) pp. 1999-2001, ISSN # 00036951

Vo-Dinh, T.; Stokes, D. L.; Wabuyele, M. B.; Martin, M. E.; Song, J. M.; Jagannathan, R.; Michaud, E.; Lee, R. J. & Pan, X. (2004). A hyperspectral imaging system for in vivo optical diagnostics. *IEEE Engineering in Medicine and Biology Magazine*, Vol. 23, No. 5, (September/October 2004) pp. 40-49, 07395175

Wang, S. S. & Magnusson, R. (1993). Theory and applications of guided-mode resonance filters. *Appl. Opt.*, Vol. 32, No. 14, (May 1993) pp. 2606-2613, 00036935

Aerospace Technologies Advancements

Edited by Thawar T. Arif

ISBN 978-953-7619-96-1

Hard cover, 492 pages

Publisher InTech

Published online 01, January, 2010

Published in print edition January, 2010

Space technology has become increasingly important after the great development and rapid progress in information and communication technology as well as the technology of space exploration. This book deals with the latest and most prominent research in space technology. The first part of the book (first six chapters) deals with the algorithms and software used in information processing, communications and control of spacecrafts. The second part (chapters 7 to 10) deals with the latest research on the space structures. The third part (chapters 11 to 14) deals with some of the latest applications in space. The fourth part (chapters 15 and 16) deals with small satellite technologies. The fifth part (chapters 17 to 20) deals with some of the latest applications in the field of aircrafts. The sixth part (chapters 21 to 25) outlines some recent research efforts in different subjects.

INTECH
open science | open minds

InTech Europe
University Campus STeP Ri
Slavka Krautzeka 83/A
51000 Rijeka, Croatia
Phone: +385 (51) 770 447
Fax: +385 (51) 686 166
www.intechopen.com

InTech China
Unit 405, Office Block, Hotel Equatorial Shanghai
No.65, Yan An Road (West), Shanghai, 200040, China
中国上海市延安西路65号上海国际贵都大饭店办公楼405单元
Phone: +86-21-62489820
Fax: +86-21-62489821

IntechOpen